CONCEPTUAL DESIGN OF A HIGH TEMPERATURE SUPERCONDUCTING SPECTROSCOPY-TYPE GANTRY SYSTEM FOR PARTICLE THERAPY*

H. Zhao[†], M. Fukuda, T. Yorita, H. Kanda, T. H. Chong, H. A. Shali, S. Matsui, K. Watanabe,
T. Imura, S. Ishihata, N. Itakura, Research Center for Nuclear Physics (RCNP), Osaka, Japan
A. Gerbershagen, J. M. Schippers[1], Particle Therapy Research Center (PARTREC),
Groningen, The Netherlands
K. P. Nesteruk, Massachusetts General Hospital and Harvard Medical School, Boston, USA
[1]also at Paul Scherrer Institute (PSI), Villigen, Switzerland

Abstract

In a particle therapy facility, accelerated particles are transported to treatment room, then delivered towards a tumor by a gantry system to acquire multiple treatment angles, so that multiple treatment angles can be used to minimize the dose in healthy tissue in vicinity of the tumor. To realize the rapid change of treatment angle, enabling stereotactic irradiations to mitigate motion effect on the dose distribution, we are designing a HTS (High Temperature Superconducting) Spectroscopy-type Gantry System. In the conception of spectroscopy-type gantry, the beam is guided to the appropriate azimuthal angle with cylindrical magnetic field surrounding the patient, and treatment angles are set only by adjusting the strength of dedicated magnets, instead of rotating a gantry with magnets of the beam transport around the patient. This method is realizing a fast change of azimuthal angle in a static gantry system. The rapid change of treatment angle also gives potential possibility of FLASH therapy. In this work, a conceptual design of a HTS Spectroscopy-type Gantry System and different methods to optimize its beam transportation to the patient will be discussed.

INTRODUCTION

Radiation therapy, also known as therapeutic radiation treatment, is a cancer treatment that employs high doses of radiation to kill cancer cells or inhibit their growth by damaging their DNA. Cancer cells with irreparably damaged DNA cease to divide and eventually die. Once these damaged cells perish, they are broken down and eliminated by the body. Radiation therapy does not destroy cancer cells immediately; it requires days or weeks of treatment before the DNA is sufficiently damaged for cancer cells to die. Subsequently, cancer cells continue to die for weeks or months following the conclusion of radiation therapy. Compared to conventional surgical and chemical therapies, radiation therapy imposes a lower burden on the patient's body and results in fewer side effects.

Gantry System

To achieve multiple treatment angles for improved dose distribution in the target area and enhanced protection of the surrounding healthy tissue, a rotating gantry system design is proposed. This system rotates around the patient, allowing for various treatment angles, thereby optimizing the dose delivered while minimizing exposure to the healthy tissue surrounding the tumor.

However, implementing a rotating gantry system presents significant challenges. Magnets are mounted on the gantry structure and rotated with a large mechanical arm, resulting in a cumbersome setup for many facilities. The substantial dimensions (8-12 meters in diameter) and masses (100-200 tons) of proton gantries [1] limit the rotational speed to one turn per minute for safety, to prevent potential collisions [2]. Additionally, the mechanical constraints of a rotating gantry limit the available treatment angles to a few preinstalled positions, potentially restricting treatment planning options in certain cases [3].

PURPOSE

To achieve compactness and rapid changes in treatment angles, enabling stereotactic irradiations to mitigate motion effects on dose distribution, we are designing a High Temperature Superconducting (HTS) Spectroscopy-type Gantry System. In this design, the beam is guided to the appropriate azimuthal angle using a cylindrical magnetic field surrounding the patient. Treatment angles are set by adjusting the strength of dedicated magnets, rather than rotating a gantry with beam transport magnets around the patient.

This method allows for a fast change of continuous azimuthal angles within a range of 180°, from the vertical upside (0° Irradiate) to the vertical downside (180° Irradiate), using a static gantry system. With a rotating treatment table set to 0° or 180°, continuous treatment angles over a 360° range are achievable. The rapid change in treatment angles also presents the potential for FLASH therapy.

The internal magnetic field strength is estimated to exceed 2T, which is challenging for common conductors to generate. Therefore, superconducting coils are deemed necessary for the design. To ensure operational reliability, which is crucial for a medical device, and to achieve higher current density in the superconducting coils, we have decided to use HTS material for the coils.
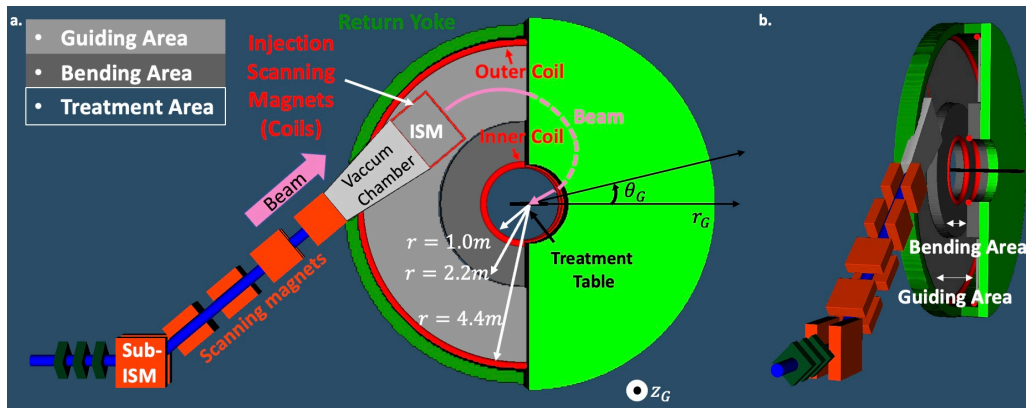
Figure 1: **a.** Front view of the designed structure of the HTS Spectroscopy-type Gantry System. Magnet poles for the guiding area and bending area are illustrated in light gray and dark gray, respectively. The treatment area is within the range of the inner coils. **b.** Side view of the structure. The pole gap in the bending area and guiding area is designed accordingly.

CONCEPTUAL DESIGN OF THE HTS SPECTROSCOPY-TYPE GANTRY SYSTEM

Structure Configuration

The structural configuration of the HTS Spectroscopy-type Gantry System is illustrated in Fig. 1. The treatment table is positioned at the center of the gantry system. The beam is transported from the left side and injected into the gantry system using an Injection Scanning Magnet (ISM), then guided to the target by the internal magnetic field. The internal magnetic field is divided into three areas: the guiding area ($r = 2.2 \sim 4.4$m), the bending area ($r = 1.0 \sim 2.2$m), and the treatment area ($r < 1.0$m). Upon injection, the beam is directed to an appropriate azimuthal angle in the guiding area, then bent toward the target in the bending area, and finally irradiates the target in the treatment area.

Magnetic fields in all areas are excited by the outer coils, while the inner coils cancel the magnetic field in the treatment area. The magnetic fields in the guiding and bending areas differ and are adjusted by the pole gap, with $2G = 30$cm in the bending area and $2G = 94$cm in the guiding area, where G is defined as half aperture of the magnet poles. The ISM sets the treatment angle by appropriately bending the beam during injection.

Internal Magnetic Field Profile Simulation

The internal magnetic field profile is simulated using Opera3D Simulation Software. The model for simulation is completely rotationally symmetric, as the ISM and vacuum chamber are not yet included in the model at this stage. Thus, we investigated the magnetic field strength with radius dependency. Figure 2 shows the outputted magnetic field profile in the midplane, from which we can calculate the trajectory of a single particle.

Particle Trajectory Calculation

To calculate particle trajectories from the ISM to the target for the designed treatment angles, we reversed the transportation and tracked a single particle starting from the target
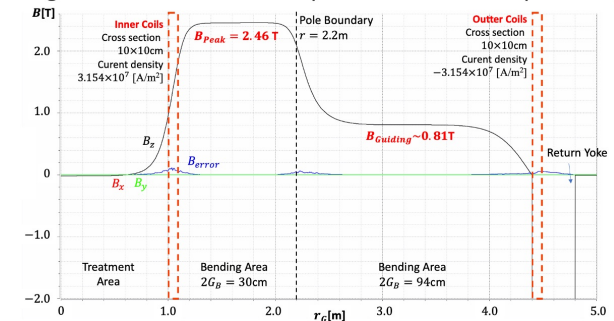

Figure 2: The magnetic field profile in the midplane was simulated using Opera3D. The peak of B_z in the bending area is approximately 2.46 T. In the guiding area, B_z remains around 0.81 T.

$(r, \theta) = (0, 0)$ to the exit of the ISM for each treatment angle. Single particle tracking in the gantry system was calculated using a self-built C program with numerical calculations based on the algorithm illustrated in Fig. 3. For rough calculations, the time step was set to $\Delta t = 5 \times 10^{-12}$ seconds, resulting in a travel distance of $\Delta Beamz = 0.9$ mm for 230 MeV protons.

To control the ISM accurately, the beam status (e.g., transportation axis and direction) at both the entrance and exit of the magnets is required. The beam status at the entrance primarily depends on the accelerator and beam line adjustments. Therefore, at this phase, we need to summarize the beam status required at the exit of the ISM to ensure that the beam follows the designed trajectory to the specified treatment angle $\theta_r T$. There are two necessary injection conditions for a designed trajectory: the radial distance $r_{injection}$ and the angle between the tangent line of the trajectory and the normal of the ISM $\varphi_{injection}$ at the exit of the ISM.

The calculated particle trajectories in the midplane of the HTS Spectroscopy-type Gantry System are illustrated in Fig. 4**a**, for treatment angles θ ranging from 0° (vertical irradiation) to 180° (vertical irradiation from the back), using
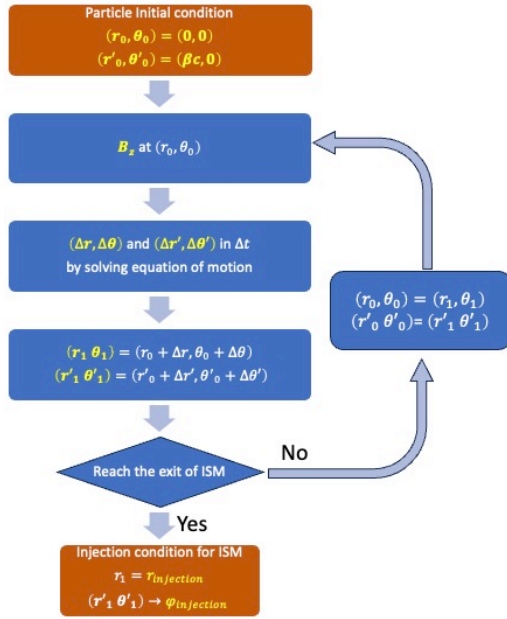
Figure 3: Algorithm of the program for tracking a single particle in the gantry system.
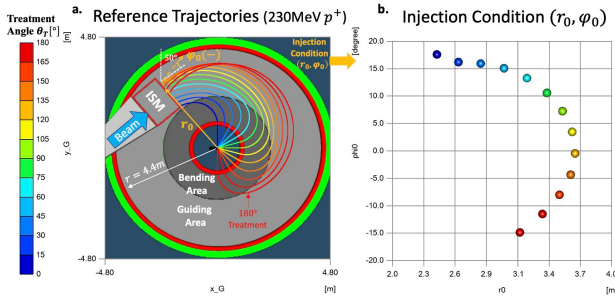

Figure 4: **a.** Reference particle trajectory in the midplane of the HTS Spectroscopy-type Gantry System for 0° to 180° treatment angle (color bar), using 230 MeV protons with numerical calculation. **b.** Injection condition (r_0, φ_0) for the treatment angle θ_T with a changing step of 15° from 0° to 180°. The horizontal axis represents r_0, and the vertical axis represents φ_0.

230 MeV protons. The beam is transported to the HTS Spectroscopy-type Gantry System from the left side and enters the ISM (Injection Scanning Magnet). The magnetic field in the ISM is controlled to direct the beam onto the trajectories designed for a certain treatment angle θ_T.

When we sum up the injection conditions (r_0, φ_0) for the treatment angle θ_T from 0° to 180°, we obtain the graph shown in Fig. 4**b**. The bubble points represent the injection conditions for each treatment angle with a step change of 15° , and the treatment angles between steps are also valid. This indicates the potential for continuous treatment angles in the range of 0° ~ 180°.

Beam Spot Size Evaluation

In an actual treatment, beam scanning technology is utilized to deliver the dose with precision. In the HTS Spectroscopy-type gantry system, we intend to implement a pencil beam scanning (PBS) system. For this system, the beam spot size is crucial, with an optimal value of approximately $\sigma \sim 5$ mm. Therefore, evaluating the beam spot size is a critical aspect in the development of the conceptual design.

Particle Source for Evaluation To evaluate the beam spot size during transportation, we tracked particles with various assumed initial conditions within a 3D magnetic field profile. Ideally, a real beam would exhibit a Gaussian distribution in both real space and phase space. However, for preliminary calculations, we tracked particles using only typical initial conditions. To distinctly describe the coordinates, we employed polar coordinates (r_G, θ_G, z_G) as the global coordinate system, as illustrated in Fig. 1. Additionally, we used a beam transportation coordinate system (x, y, z), where z represents the beam transportation direction.
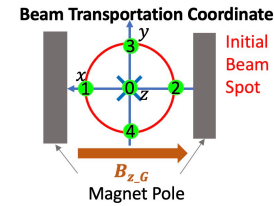

Figure 5: Beam spot in beam transportation coordinate.

Figure 5 illustrates a beam spot in real space using the beam transportation coordinates, assuming identical initial conditions in both the bending plane and the non-bending plane. In this scenario, we simply track particles at the central point and those at the edge of the beam envelope in both planes, specifically at positions 0 and 1 through 4 as shown in Fig. 5.

We then listed the typical conditions for particles at each position in Table 1, taking into account the beam phase space and momentum spread. For example, at position 1, when the initial offset Δx is taken as $\sqrt{\epsilon_x \beta_x}$, the initial deviation $\Delta x'$ must be 0 due to the envelope in phase space. Conversely, in the y plane, the initial offset Δy is taken as 0, and thus the initial deviation $\Delta y'$ varies within the range of $-\sqrt{\epsilon_y \gamma_y}$ to $+\sqrt{\epsilon_y \gamma_y}$. We tracked particles with 5 initial deviations: $-\sqrt{\epsilon_y \gamma_y}, -0.5\sqrt{\epsilon_y \gamma_y}, 0, +0.5\sqrt{\epsilon_y \gamma_y}, +\sqrt{\epsilon_y \gamma_y}$. Additionally, the initial momentum spread was considered in 5 steps: $0, \pm\Delta\frac{P}{P_0}, \pm0.5\Delta\frac{P}{P_0}$. Combining these with the 5 initial deviations, we observed 5×5 different initial conditions at position 1. Applying this method to all 5 positions, we obtained a total of $125 + 25 \times 4$ different initial conditions (since the deviation of particles at position 0 varies in both x and y planes, resulting in 125 variations).

Assumed beam parameters of emittance, TWISS parameters, momentum spread, and dispersion function in both the bending plane and the non-bending plane are listed in Table 2,

Table 1: Initial Conditions for Particles at Each Position

Typical Condition at Each Position					
Position	0	1	2	3	4
Δx	0	$+\sqrt{\epsilon_x \beta_x}$	$-\sqrt{\epsilon_x \beta_x}$	0	0
$\Delta x'$	$0, \pm\sqrt{\epsilon_x \gamma_x},$ $\pm 0.5\sqrt{\epsilon_x \gamma_x}$	0	0	$0, \pm\sqrt{\epsilon_x \gamma_x},$ $\pm 0.5\sqrt{\epsilon_x \gamma_x}$	$0, \pm\sqrt{\epsilon_x \gamma_x},$ $\pm 0.5\sqrt{\epsilon_x \gamma_x}$
Δy	0	0	0	$+\sqrt{\epsilon_y \beta_y}$	$-\sqrt{\epsilon_y \beta_y}$
$\Delta y'$	$0, \pm\sqrt{\epsilon_y \gamma_y},$ $\pm 0.5\sqrt{\epsilon_y \gamma_y}$	$0, \pm\sqrt{\epsilon_x \gamma_y}$ $\pm 0.5\sqrt{\epsilon_x \gamma_y}$	$0, \pm\sqrt{\epsilon_x \gamma_y}$ $\pm 0.5\sqrt{\epsilon_x \gamma_y}$	0	0
$\Delta \frac{p}{p_0}$	$0, \pm\Delta\frac{p}{p_0}, \pm 0.5\Delta\frac{p}{p_0}$				

Table 2: Assumed Initial Beam Parameters in both Bending and Non-bending Plane for Beam Spot Size Evaluation

Initial Parameters	
Parameters	Value
ϵ_0	$10^{-6}\pi \cdot$m$\cdot$rad
β_0	9.0 m
α_0	0
γ_0	0.11 rad
$(\Delta p/p_0)_0$	1%
D_0	0 m

considering a 230 MeV proton accelerated by a cyclotron and then decelerated with a degrader. The beam envelope in phase space can be calculated, which is Δu_{max} = 3 mm and $\Delta u'_{max}$ = 0.33 mrad.

3D Magnetic Field Profile   The magnetic field is simulated using Opera3D. We used only B_{zG} in the mid-plane for reference trajectory calculations because no initial offset or deviation in the z_G direction is considered there. However, to evaluate the beam spot size, the 3D magnetic field profile $\mathbb{B} = (B_{rG}, B_{\theta G}, B_{zG})$ in the global coordinates (r_G, θ_G, z_G) is required. Thus, we output the magnetic field profile $\mathbb{B}(r_G, \theta_G)$ in $r_G\theta_G$ planes at $z = 0, 5, 10, 15$ mm, with a step size of $\Delta r_G = 5$ mm and $\Delta\theta_G = 0.5°$ in each plane. In particle tracking, magnetic field correction is applied using linear terms in all three directions of (r_G, θ_G, z_G).

Particle Tracking   Particle tracking in the gantry system is calculated using a self-built C program with numerical calculations based on the algorithm illustrated in Fig. 6, with a time step of $\Delta t = 5 \times 10^{-12}$ s. The initial conditions of the particles are determined by the injection conditions illustrated in Fig. 4**b**, as well as the assumed initial conditions and beam parameters listed in Table 1 and Table 2. Although the initial conditions are assumed to be the same for all treatment angles, beam focusing during transportation may perform differently. Therefore, we calculated the transportation for the 180° treatment angle, which has the longest transportation distance.
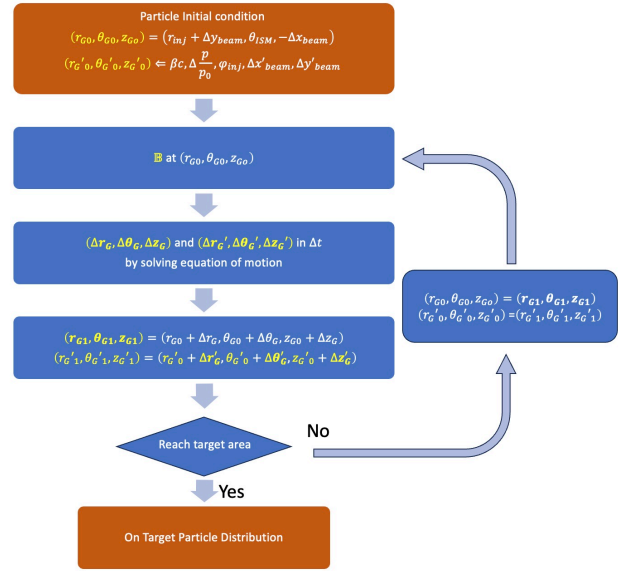

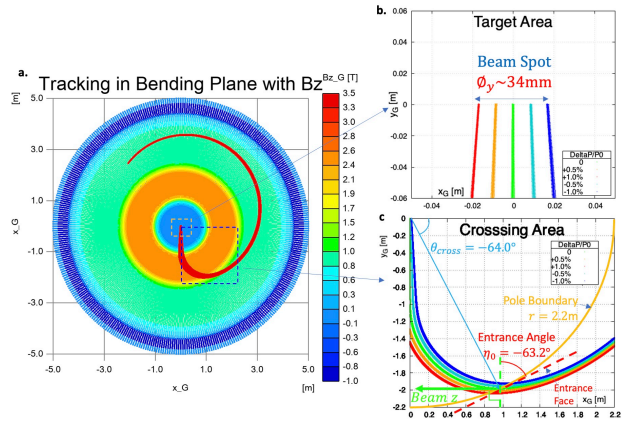Figure 6: Algorithm of the program for tracking particles in the gantry system.

Figure 7: **a.** Particle tracking in the gantry system for 180° treatment. Color represents the magnetic field strength B_{zG}. **b.** Enlarged view of the target area. Particles with different momentum spreads are plotted in different colors. **c.** Enlarged view of the target area where particles cross the pole boundary.

The particle tracking result in the bending plane is illustrated in Fig. 7. An overview of the transportation in the gantry with the magnetic field strength B_{zG} is shown in Fig. 7**a**. The target area is enlarged in Fig. 7**b**, where particle trajectories right before hitting the target can be observed. The diameter of the on-target beam spot size in the bending plane is calculated to be 34 mm, which is clearly too large for the PBS system. From the trajectory plot, we can see that the beam defocusing is mainly due to momentum spread, which is our primary concern. To investigate why the beam is heavily defocused in the bending plane, we examined the area where particles cross the pole boundary ($r_G = 2.2$ m) (Fig. 7**c**). The angle between the entrance face and the beam transportation direction is defined as the entrance angle η_0, as commonly used in the calculation of a wedge magnet. The particle tracking result shows that the entrance angle of particles with a momentum spread $(\Delta p/p_0)_0 = 0$ is $\eta_0 = -63.2°$, which generally causes significant defocusing in the bending area [4].

Sawtooth Shaping on Magnet Poles Facing the issue of beam defocusing in the bending plane due to momentum spread, we plan to implement a sawtooth shaping at the pole boundary. This modification aims to decrease the entrance angle η_0, thereby reducing the defocusing effect in the bending plane.
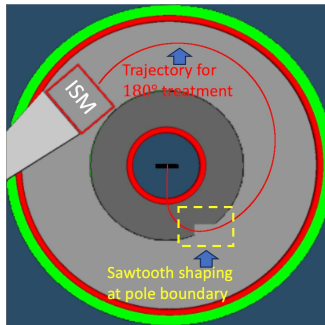

Figure 8: Sawtooth shaping at the boundary of magnet pole.

As illustrated in Fig. 8, based on the reference trajectory for the 180° treatment angle, we implemented a sawtooth shaping at the magnet pole boundary where the particle with $(\Delta p/p_0)_0 = 0$ crosses $r_G = 2.2$ m. As mentioned in the structural introduction, the pole gap in the bending area and guiding area is 30 cm and 94 cm, respectively. In the sawtooth area, we modified the magnet so that the sawtooth shaping in the bending area increases the pole gap in the sawtooth area to 94 cm, matching the guiding area.

The magnetic field with sawtooth shaping was simulated using Opera3D, and the magnetic field profile B_{zG} is illustrated in Fig. 9**a**. Point 0 refers to the point where the reference trajectory crosses the magnet pole boundary, with the entrance designed to be 15 cm inward and 10 cm outward. We then calculated the injection condition in the new magnetic field profile for the 180° treatment angle using the program for tracking a single particle (algorithm illustrated
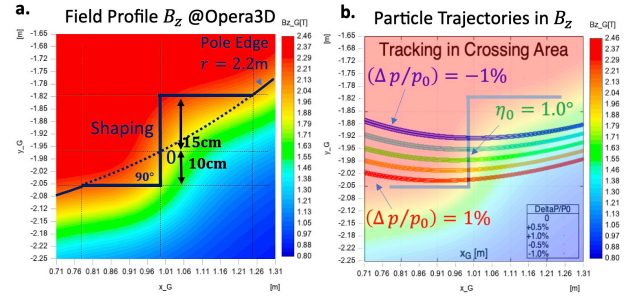

Figure 9: **a.** Magnetic field profile B_{zG} in the shaping area. **b.** Particle trajectories crossing the shaping area.

in Fig. 3). We tracked the particles in the gantry with the new injection condition and the same beam initial parameters listed in Table 2. The sawtooth shaping is intended to cover all particles within the entrance face; otherwise, critical beam defocusing or even massive particle loss may occur. Therefore, we plotted the particle trajectories in the shaping area (Fig. 9**b**) and observed that all particles within a momentum spread of $(\Delta p/p_0)_0 = -1\% \sim 1\%$ crossed the entrance face. The entrance angle was approximately $\eta_0 = -1.0°$.
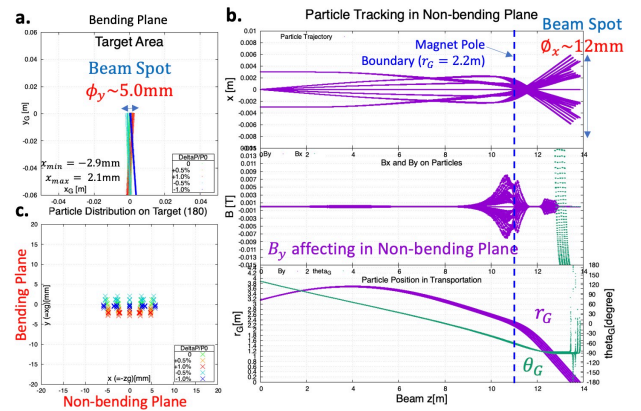

Figure 10: **a.** Enlarged view of the target area in the bending plane. Particles with different momentum spreads are plotted in different colors. **b.** Beam transportation in the non-bending plane. The horizontal axis represents the transportation distance. The vertical axes represent the particle offset in the non-bending plane, the magnetic field strength perpendicular to the non-bending plane, and the particle position in the (r_G, θ_G) plane. **c.** On-target particle distribution.

The particle tracking results in both bending and non-bending planes are illustrated in Fig. 10. The target area is enlarged in Fig. 10**a**, where particle trajectories right before hitting the target can be observed. The diameter of the on-target beam spot size in the bending plane is calculated to be 5.0 mm, which is suitable for a general PBS system. Beam transportation in the non-bending plane is illustrated in Fig. 10**b**. The beam became heavily over-focused while crossing the boundary of the magnet pole and finally defo-

cused on the target. The particle distribution on the target is illustrated in Fig. 10**c**. With the sawtooth shaping at the boundary of the magnet poles, we successfully reduced the beam spot diameter in the bending plane from 34 mm to 5.0 mm, and the beam spot diameter in the non-bending plane is estimated to be 12 mm.

CONCLUSION

To realize the compactness and rapid change of treatment angles, enabling stereotactic irradiations to mitigate motion effects on dose distribution, we are designing a High Temperature Superconducting (HTS) Spectroscopy-type Gantry System. We have calculated the reference particle trajectories and injection conditions for treatments from 0° to 180° by tracking a single particle in a simulated magnetic field, using a self-built C program with numerical calculations.

To evaluate the on-target beam spot size, we tracked 225 particles under different initial conditions with assumed beam initial parameters and simulated 3D magnetic field profiles for the 180° treatment angle. This was done using a self-built C program based on numerical calculations and calculated injection conditions. The results indicate that the beam may become heavily defocused during transportation, with the diameter of the on-target beam spot estimated to be 34 mm in the bending plane.

Facing the beam focusing problem, we tried sawtooth shaping at the boundary of the magnet poles, which is similar to constructing a wedge magnet in beam transportation. With the sawtooth shaping, the on-target beam spot is estimated to be reduced to 5.0 mm in the bending plane and 12 mm in the non-bending plane.

In the design of a wedge magnet, generally, the magnetic field outside the magnet is hardly considered. However, in this work, the wedge magnet (i.e., sawtooth shaping) is installed in a bending magnet, so the fringe field of the wedge magnet is difficult to evaluate or even approximate to a hard edge for calculation. Thus, as a potential solution to the beam focusing problem in this work, the sawtooth shaping method still requires more data for focusing length calculation, considering the dependency on the entrance face length and entrance angle.

REFERENCES

[1] M. E. Schulze, "Commissioning results of the LLUMG beam switchyard and gantry", in *Proceedings of the 14th Particle Accelerator Conference (PAC'91)*, 1991, pp. 610-613.

[2] G. Nicolini *et al.*, "On the impact of dose rate variation upon RapidArc implementation of volumetric modulated arc therapy", *Medical Physics*, **38**, 2011, 264-271.

[3] K. P. Nesteruk *et al.*, "Title of the paper", *Physics in Medicine & Biology*, **66**, 2021, 055018.

[4] H. Wiedemann, *Particle Accelerator Physics* (Fourth Edition), Springer, 2015.